

Dual catalytic performance of arene-ruthenium amine complexes for norbornene ring-opening metathesis and methyl methacrylate atom-transfer radical polymerizations

Thais R. Cruz¹ | Eliada A. Silva² | Douglas P. Oliveira¹ | Daniele M. Martins² |
Patrik D.S. Gois¹ | Antonio E.H. Machado^{3†} | Pedro Ivo S. Maia⁴ |
Beatriz E. Goi¹ | Benedito S. Lima-Neto² | Valdemiro P. Carvalho-Jr¹

¹Faculdade de Ciências e Tecnologia,
UNESP – Univ. Estadual Paulista, CEP
19060-900, Presidente Prudente, SP, Brazil

²Instituto de Química de São Carlos,
Universidade de São Paulo, CEP
13560-970, São Carlos, SP, Brazil

³Instituto de Química, Universidade
Federal de Uberlândia, P.O. Box 593,
Uberlândia, 38400-089, Minas Gerais,
Brazil

⁴Departamento de Química, Universidade
Federal do Triângulo Mineiro, CEP
38025-440, Uberaba, MG, Brazil

Correspondence

Valdemiro P. Carvalho-Jr, Faculdade de
Ciências e Tecnologia, UNESP – Univ.
Estadual Paulista, CEP 19060-900,
Presidente Prudente, SP, Brazil.
Email: valdemiro.carvalho@unesp.br

Benedito S. Lima-Neto, Instituto de
Química de São Carlos, Universidade de
São Paulo, CEP 13560-970, São Carlos, SP,
Brazil.
Email: benedito@iqsc.usp.br

Funding information

FAPESP, Grant/Award Numbers:
2017/06329-5, 2018/06340-1

Arene ruthenium(II) complexes bearing the cyclic amines $\text{RuCl}_2(\eta^6\text{-}p\text{-cymene})(\text{pyrrolidine})$ (**1**), $[\text{RuCl}_2(\eta^6\text{-}p\text{-cymene})(\text{piperidine})]$ (**2**), and $[\text{RuCl}_2(\eta^6\text{-}p\text{-cymene})(\text{peridroazepine})]$ (**3**) were successfully synthesized. Complexes **1–3** were fully characterized by means of Fourier transform infrared, UV-visible, and NMR spectroscopy, elemental analysis, cyclic voltammetry, computational methods, and one of the complexes was further studied by single crystal X-ray crystallography. These compounds were evaluated as catalytic precursors for ring-opening metathesis polymerization (ROMP) of norbornene (NBE) and atom-transfer radical polymerization (ATRP) of methyl methacrylate (MMA). NBE polymerization via ROMP was evaluated using complexes **1–3** as pre-catalysts in the presence of ethyl diazoacetate (EDA) under different [NBE]/[EDA]/[Ru] ratios, temperatures (25 and 50°C), and reaction times (5–60 min). The highest yields of polyNBE were obtained with [NBE]/[EDA]/[Ru] = 5000/28/1 for 60 min at 50°C. MMA polymerization via ATRP was conducted using **1–3** as catalysts in the presence of ethyl- α -bromoisobutyrate (EBiB) as initiator. The catalytic tests were evaluated as a function of the reaction time using the initial molar ratio of [MMA]/[EBiB]/[Ru] = 1000/2/1 at 95°C. The increase in molecular weight as function of time indicates that complexes **1–3** were able to mediate the MMA polymerization with an acceptable rate and some level of control. Differences in the rate of polymerization were observed in the order **3 > 2 > 1** for the ROMP and ATRP.

KEY WORDS

ATRP, olefin, *p*-cymene, ROMP, ruthenium

[†]During his stay as Visiting Professor at the Programa de Pós-Graduação em Ciências Exatas e Tecnológicas at Universidade Federal de Goiás, Catalão, Goiás, Brazil

1 | INTRODUCTION

Living polymerization techniques have been traditionally employed for the synthesis of block copolymers through a combination of distinct polymerization methods where two or more monomers are polymerized sequentially or simultaneously via tandem catalysis. Ring-opening metathesis (ROMP) and atom-transfer radical (ATRP) polymerizations are two of the most widely used polymerization methods in synthetic polymers that can be combined to synthesize new polymeric materials with controlled design and architecture.^[1–8]

As a direct result of this interest in ROMP and ATRP applications, several active ruthenium catalysts were developed for these catalytic reactions. The ruthenium-based catalyst systems have been demonstrated to be effective for initiating the ROMP of a variety of cyclic olefins and as mediators for ATRP of vinyl monomers.^[9–13] Among these catalysts, arene-ruthenium compounds are of great importance in both reactions. Ruthenium complexes bearing *p*-cymene with different types of ligands such as phosphines,^[14–16] Schiff bases,^[17,18] and *N*-heterocyclic carbenes^[19–22] with a general formula of $[\text{RuCl}_2(\text{p-cymene})(\text{L})]$ have been investigated as ROMP or ATRP catalysts. In our research group, noncarbene ruthenium-based complexes have been studied for ROMP and ATRP.^[22–40] Many of these compounds have exhibited good activity, forming polymers and copolymers in high yields, with different thermal and morphological characteristics. Among these precatalysts, ruthenium amine compounds have produced polymers from norbornene (NBE) and norbornadiene (NBD) by ROMP and controlled methyl methacrylate (MMA) and styrene (St) polymerization via ATRP. The electronic combination of a transition metal with a σ -donor amine has been a convenient modular approach to tune the reactivity of such initiators when varying its moiety.

In this study, we report the application of $[\text{RuCl}_2(\text{p-cymene})(\text{amine})]$ complexes, with amine = pyrrolidine (**1**), piperidine (**2**), or perhydroazepine (**3**), as catalyst precursors for ROMP of NBE and ATRP of MMA under different conditions of temperature, reaction time, and $[\text{Ru}]/[\text{monomer}]/[\text{initiator}]$ ratio. The purpose was to observe the influence of the *p*-cymene ligand on the reactivity of ruthenium catalysts bearing different cyclic amines, interpreting the subtle changes in the electronic and steric parameters of the catalytic systems to obtain resources to understand the features that influence ROMP and ATRP efficiency. To the best of our knowledge, this is the first study in the literature that systematically investigated the effect of different cyclic amines on the efficiency of arene-ruthenium compounds as promising dual catalysts for ROMP and ATRP.

2 | EXPERIMENTAL

2.1 | General remarks

Unless otherwise stated, all syntheses and manipulations were performed under nitrogen atmosphere following standard Schlenk techniques. Solvents were distilled from appropriate drying agents and deoxygenated prior to use. MMA was washed with 5% NaOH solution, dried over anhydrous MgSO_4 , vacuum distilled from CaH_2 , and stored under nitrogen at -18°C before use. 2,2,6,6-tetramethyl-1-piperidinoxyl (TEMPO), ferrocene (Fc), (NBE, ethyl diazoacetate (EDA), pyrrolidine (pop), piperidine (pip), perhydroazepine (pep), alpha-terpinene, and ethyl 2-bromoisobutyrate (EBiB) were obtained from Aldrich and used as acquired. The $[\text{RuCl}_2(\text{p-cymene})]_2$ and $[\text{RuCl}_2(\text{p-cymene})(\text{piperidine})]$ complexes were prepared following the literature and their purity was checked by satisfactory elemental analysis and spectroscopic examination (NMR, Fourier transform infrared [FT-IR] spectroscopy and Electron Paramagnetic Resonance [EPR]).^[40,41]

2.2 | Analyses

Elemental analyses were performed with a Perkin-Elmer (Waltham, Massachusetts, USA) CHN 2400 instrument. Infrared spectra were obtained on a Perkin Elmer Frontier instrument equipped with a diamond Attenuated total reflection module. The electronic spectra were recorded on a Shimadzu (model UV-1800, Nakagyo-ku, Kyoto, Japan) spectrophotometer, using 1 cm path length quartz cells. The ^1H and $^{13}\text{C}\{^1\text{H}\}$ NMR spectra were obtained in CDCl_3 at 298 K on a Bruker (Billerica, Massachusetts, USA) DRX-400 spectrometer operating at 400.13 and 100.62 MHz, respectively. The chemical shifts are listed in parts per million downfield from Tetramethylsilane (TMS) and are referenced from the solvent peaks or TMS. The conversions were determined from the concentration of residual monomer measured by gas chromatography (GC) using a Shimadzu GC-2010 gas chromatograph equipped with a flame ionization detector and a 30 m (0.53 mm internal diameter, 0.5 μm film thickness) SPB-1 Supelco (Bellefonte, Pennsylvania, USA) fused silica capillary column. Anisole was added to polymerization and used as an internal standard. Analysis conditions: injector and detector temperature 250°C ; temperature program 40°C (4 min), $20^\circ\text{C}/\text{min}$ until 200°C , 200°C (2 min). The molecular weights and the molecular weight distribution of the polymers were determined by gel permeation chromatography using a Shimadzu Prominence LC system equipped with a LC-20 AD pump, a

DGU-20A5 degasser, a CBM-20A communication module, a CTO-20A oven at 40°C, and a RID-10A detector equipped with two Shimadzu columns (GPC-805: 30 cm, \varnothing = 8.0 mm). The retention time was calibrated with poly(methyl methacrylate) standards using HPLC-grade Tetrahydrofuran (THF) as an eluent at 40°C with a flow rate of 1.0 ml/min. Electrochemical measurements were performed using an Autolab PGSTAT204 potentiostat with a stationary platinum disk and a wire as working and auxiliary electrodes, respectively. The reference electrode was Ag/AgCl. The measurements were performed at 25°C ± 0.1 in CH₂Cl₂ with 0.1 mol/L of *n*-Bu₄NPF₆.

2.3 | General procedure for the preparation of Ru complexes

An oven-dried 50 ml Schlenk flask equipped with a magnetic stirring bar and capped with a rubber septum containing 0.350 g (0.57 mmol) of the [{RuCl₂(*p*-cymene)}₂] was purged of air by applying three vacuum/argon cycles before the addition of dry 30 ml of CH₂Cl₂ and 2 equivalents of the desired amine (pop, pip or pep). Immediately after the addition, an orange solution formed and the reaction mixture was stirred for 4 hr at 65°C under reflux. Finally, the solvent was evaporated under vacuum till dryness. The residue was washed with ether (20 ml) and dried under high vacuum, affording an orange precipitate.

2.3.1 | [RuCl₂(*p*-cymene)(pop)] (1)

Yield 332 mg (77%). Anal. calcd for C₁₄H₂₃Cl₂NRu: C 44.57, H 6.14, N 3.71%; found: C 44.34, H 5.95, N 3.68%. UV-Vis $\lambda_{\text{max}}/\text{nm}$ ($\epsilon_{\text{max}} [\text{M}^{-1}, \text{cm}^{-1}]$): 338 (0.33), 408 (0.26). FT-IR (CsI, cm⁻¹): ν N-H (3267), ν C-H sp² (3042), ν C-H sp³ (2963, 2861), ν Ru-Cl (346, 311). ¹H NMR (400 MHz, CDCl₃, δ/ppm): 1.30 (d, *J* = 7.2 Hz, 6H, -CH(CH₃)₂, *p*-cym), 1.61–1.92 (m, 4H, CH₂, pop), 2.24 (s, 3H, CH₃, *p*-cym), 2.68 (s, 1H, NH, pop), 2.77–2.91 (m, 2H, pop), 3.62–3.72 (m, 2H, CH₂, pop), 3.02 (sept, *J* = 7.2 Hz 1H, CH-(CH₃)₂, *p*-cym), 5.26 (s, 4H, *p*-cym CH_{ar}). ¹³C NMR (100 MHz, CDCl₃): 18.37, 22.0, 24.57, 30.92, 55.16, 78.67, 82.80, 93.47, 104.28 ppm. EPR: no signal was observed.

2.3.2 | [RuCl₂(*p*-cymene)(pip)] (2)

Yield 300 mg (67%). Anal. calcd for C₁₅H₂₅Cl₂NRu: C 46.04, H 6.44, N 3.58%; found: C 45.95, H 6.34, N 3.52%. UV-Vis $\lambda_{\text{max}}/\text{nm}$ ($\epsilon_{\text{max}} [\text{M}^{-1}, \text{cm}^{-1}]$): 338 (0.36); 406 (0.26). FT-IR (CsI, cm⁻¹): ν N-H (3246), ν C-H sp² (3049), ν C-H sp³ (2947, 2867), ν Ru-Cl (346, 310). ¹H

NMR (400 MHz, CDCl₃, δ/ppm): 1.30 (d, *J* = 6.0, 6H, CH(CH₃)₂, *p*-cym), 1.38–2.19 (m, 7H, CH₂ + NH, pip), 2.22 (s, 3H, CH₃, *p*-cym), 1.87–2.97 (qd, *J* = 7.6 Hz, *J* = 1.6 Hz, 2H, CH₂, pip), 3.02 (sept, *J* = 6.0 Hz, 1H, *p*-cym CH(CH₃)₂), 3.82 (d, *J* = 10 Hz, 2H, CH₂, pip), 5.28 (d, *J* = 5.0 Hz, 2H, *p*-cym CH_{ar}), 5.33 (d, *J* = 5.0 Hz, 2H, *p*-cym CH_{ar}). ¹³C NMR (100 MHz, CDCl₃, δ/ppm): 18.21, 21.95, 23.90, 28.88, 30.82, 55.65, 77.96, 83.09, 92.68, 104.54 ppm. EPR: no signal was observed.

2.3.3 | [RuCl₂(*p*-cymene)(pep)] (3)

Yield 315 mg (68%). Anal. calcd for C₁₆H₂₇Cl₂NRu: C 47.41, H 6.71, N 3.46%; found: C 47.78, H 6.48, N 3.41%. UV-Vis $\lambda_{\text{max}}/\text{nm}$ ($\epsilon_{\text{max}} [\text{M}^{-1}, \text{cm}^{-1}]$): 340 (0.34); 408 (0.26). FT-IR (CsI, cm⁻¹): ν N-H (3246), ν C-H sp² (3054), ν C-H sp³ (2933, 2846), ν Ru-Cl (346, 310). ¹H NMR (400 MHz, CDCl₃, δ/ppm): 1.31 (d, *J* = 7.2, 6H, *p*-cym CH(CH₃)₂), 1.49–1.71 (m, 9H, CH₂ + NH, pep), 2.21 (s, 3H, CH₃, *p*-cym), 3.04 (sept, *J* = 7.2 Hz, 1H, CH₂), 3.82 (d, 2H, CH₂ pep), 5.29 (d, *J* = 6.4 Hz, 2H *p*-cym CH_{ar}), 5.33 (d, *J* = 6.4 Hz, 2H *p*-cym CH_{ar}). ¹³C NMR (100 MHz, CDCl₃, δ/ppm): 18.33, 22.04, 25.74, 30.81, 31.00, 57.92, 78.21, 82.95, 92.67, 104.43 ppm. EPR: no signal was observed.

2.4 | Crystal structure determination

Orange crystals of **3** were grown by slow evaporation from a CH₂Cl₂ solution at room temperature. The data collections were performed using Mo-Kα radiation (*i* = 71.073 pm) on a Bruker Apex II Duo diffractometer. Standard procedures were applied for data reduction and absorption correction.^[42,43] Structure solution and refinement were performed with the SHELX program package^[44,45] and all non-hydrogen atoms were refined with anisotropic displacement parameters. Hydrogen atoms were placed at calculated positions and treated with the “riding model” option of SHELXL. The methylene groups from the hexamethyleneimine of one of the molecules in the asymmetric unit are disordered with occupancies 0.807:0.193. The C-C and C-N bond distances for the disordered part were fixed using the DFIX command of SHELX. More details on data collections and structure determination are given in Table 1. ORTEP-3 was employed for molecular graphics.^[46]

2.5 | Computation details

The structures of the compounds under study were optimized and their vibrational frequencies were calculated

TABLE 1 Crystal data and structure refinement for complex **3**

Parameters	3
Empirical formula	C ₁₆ H ₂₇ Cl ₂ NRu
Formula weight	405.35
Temperature (K)	296(2)
Wavelength (Å)	0.71073
Crystal system	Monoclinic
Space group	P2 ₁ /n
<i>a</i> (Å)	12.8893(7)
<i>b</i> (Å)	14.9977(7)
<i>c</i> (Å)	18.6020(10)
β (°)	95.688(2)
<i>V</i> (Å) ³	3578.2(3)
<i>Z</i>	8
<i>D</i> _{calc} (mg/m)	1.505
Absorption coefficient (mm ⁻¹)	1.166
θ range for data collection (°)	1.748–26.401
Crystal size (mm ³)	0.506 × 0.305 × 0.089
Number of reflections collected	71224
Number of independent reflections/ <i>R</i> _{int}	7323/0.0255
Data/restraints/no. of parameters	7323/14/392
Final <i>R</i> indices [<i>I</i> > 2σ(<i>I</i>)]	<i>R</i> ₁ = 0.0263, <i>wR</i> ₂ = 0.0506
<i>R</i> indices (all data)	<i>R</i> ₁ = 0.0347, <i>wR</i> ₂ = 0.0574
GOF	1.145
Largest difference peak and hole (eÅ ⁻³)	0.466 and -0.385
CCDC code	1966839

using the density functional theory (DFT) at the level of the functional M06,^[46] implemented in Gaussian 09,^[47] using the basis set DGDZVP.^[48] The presence of the solvent in the optimizations was simulated using the IEFPCM model.^[49] From the analysis of the thermodynamic parameters obtained by the analysis of the vibrational spectra of the complexes and their different possible intermediates, it was possible to evaluate the ROMP mechanism initiated by the complexes **1–3**.

2.6 | ROMP procedure

In a typical ROMP experiment, 1.1 μmol of complex was dissolved in CHCl₃ (2 ml) with an appropriate amount of monomer (NBE), followed by addition of carbene source (EDA). The polymerization was performed for different periods of time (5–60 min). The reaction mixture was

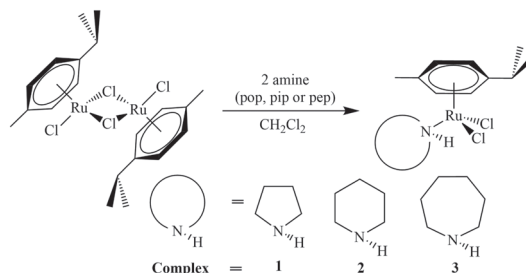
stirred at 25 or 50°C in a silicon oil bath. At room temperature, 10 ml of methanol was added and the precipitated polymer was filtered, washed with methanol, and dried in a vacuum oven at 40°C up to constant weight. The reported yields are average values from catalytic runs performed at least three times and the listed values are the arithmetic averages. The isolated polyNBEs were dissolved in THF for GPC data.

2.7 | ATRP procedure

In a typical ATRP experiment, 12.3 μmol of complex was placed in a Schlenk tube containing a magnet bar and capped by a rubber septum. Air was expelled by three vacuum–nitrogen cycles before appropriate amounts of monomer (MMA), initiator (EBiB), and toluene (1 ml) were added. All liquids were handled with dried syringes under nitrogen. The tube was capped under N₂ atmosphere using Schlenk techniques, then the reaction mixture was immediately immersed in an oil bath previously heated to the desired temperature. The polymerizations were conducted at 95°C. The samples were removed from the tube after certain time intervals using degassed syringes. The polymerization was stopped when the reaction mixture became very viscous. The reported conversions are average values from catalytic runs performed at least twice.

3 | RESULTS AND DISCUSSION

Ligand–ruthenium arene compounds are of great importance owing to their ease of synthesis, exceptional stability, and catalytic variety. In this study, amine–ruthenium arene complexes were synthesized from one-pot synthesis between the desired amine and [RuCl₂(*p*-cymene)]₂ in CH₂Cl₂ (Scheme 1). After 4 hr of reaction, the solution containing the product was evaporated under vacuum and complexes **1–3** were obtained as a fine orange precipitate. The isolated products reached good yields (67–77%).



S C H E M E 1 Synthesis protocol of the arene–Ru^{II} complexes bearing cyclic amines **1–3**

and their compositions and structures have been well described by elementary analysis, X-ray diffraction (XRD), FT-IR, UV-visible (UV-Vis), NMR, and computational studies. Additional characterizations of complex $[\text{RuCl}_2(p\text{-cymene})(\text{pip})]$ (**2**) was discussed in order to complete the early presented studies and to better understand its reactivity in the current purpose.^[40]

Complexes **1–3** exhibited almost identical FT-IR, UV-Vis, and NMR spectra, which is consistent with the fact that they have similar structures of η^6 -*p*-cymene-Ru(II)Cl₂-amine. Typical vibration bands in the FT-IR spectra of the complexes confirm the presence of amine and *p*-cymene ligands in the isolated compounds (Supporting Information Figure S1). The bands in the region 3247–3054 cm^{−1} are attributed to $\nu(\text{N-H})$ and $\nu(\text{C-H})$ stretching of the amine and aromatic ring, respectively. Two bands observed around 345 and 310 cm^{−1} were attributed to $\nu(\text{Ru-Cl})$ asymmetric and symmetric stretching vibrations, respectively, suggesting two *cis*-positioned Cl[−] ligands. The ¹H NMR spectra of complexes **1–3** recorded in CDCl₃ solutions are shown in Supporting Information Figure S2. The presence of the *p*-cymene ligand was confirmed by the appearance of singlet and doublet peaks related to the methyl and isopropyl groups at around 2.2 and 1.3 ppm, respectively. In addition, the signal of the CH from the isopropyl is observed as a septet at 3.02 ppm. Interestingly, the signals of the aromatic hydrogen atoms appear in the range from 5.26 to 5.30 ppm, showing a shielding effect caused by the ruthenium(II) metal center when compared to the chemical shifts of typical aromatic hydrogen atoms. All the complexes show multiplets in the region of 1.4–4.0 ppm due to the presence of the methylene groups from the cyclic amines. In the ¹³C{¹H} NMR spectra, all the chemical shifts are observed in the expected regions (Supporting Information Figure S3).

The solid-state structure of $[\text{RuCl}_2(p\text{-cymene})(\text{pep})]$ (**3**) was determined by single crystal XRD analysis. The complex crystallizes in the monoclinic *P2*₁/*n* space group. The asymmetric unit contains two molecules, one of them with a considerable disorder for CH₂ groups (occupancies 0.807:0.193). The disordered part of the molecule is not discussed in this study because of the inherent uncertainties. The molecular structure of complex **3** along with atom labeling scheme is shown in Figure 1. Selected bond parameters are presented in Table 2. The crystal structure of this complex consists of an arene ring bonded to the ruthenium along with two chlorido and one amine ligands. The *p*-cymene ligand is bonded to the ruthenium atom in η^6 -fashion with Ru(II) metal ion at 1.6633(10) Å from centroid of the ring, where the Ru-C_(1–6)(*p*-cymene) bond lengths are in a relatively narrow range of 2.162(2)–2.196(2) Å. The complex adopts a typical three-legged

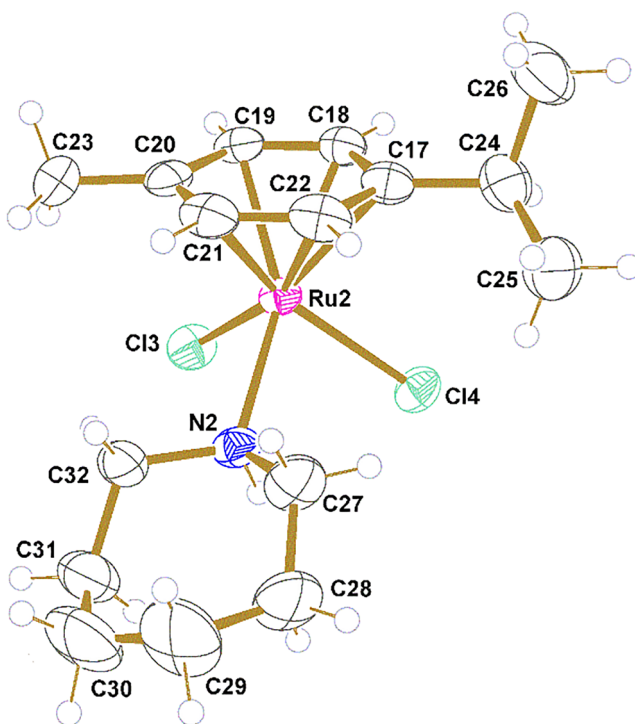


FIGURE 1 Ellipsoid plot of the complex $[\text{RuCl}_2(p\text{-cymene})(\text{pep})]$ (thermal ellipsoids at 50% of probability). Only one of the two molecules in the asymmetric unit is shown

piano stool conformation with one N and two Cl atoms as the legs. The Ru(1)–N(1) bond length for the heterocyclic N-donor is 2.174(2) Å, while the Ru–Cl bond lengths are found to be 2.4164(7) and 2.4179(7) Å for Ru(1)–Cl(1) and Ru(1)–Cl(2), respectively. The Cl–Ru–Cl bond angle is 86.82(3) $^\circ$, while the Cl–Ru–N bond angles are 81.80(6) $^\circ$ and 82.35(6) $^\circ$ for N(1)–Ru1–Cl1 and N(1)–Ru1–Cl2, respectively. Ideally, the sum of all three L–M–L angles should be equal to 270 $^\circ$, considering each L–M–L angle as 90 $^\circ$, for a perfect octahedral complex. In the case of complex **3** this sum is 251 $^\circ$, which indicates a prismatic geometry. Since all the complexes display similar spectral properties, complexes **1** and **2** are assumed to have the same structure as **3**. In fact, the crystal structure of $[\text{RuCl}_2(\eta^6\text{-p-cymene})(\text{piperidine})]$ (**2**) was previously reported,^[40] showing similar bond lengths and angles to those of **3**. However, computational studies were performed to compare their structures and other properties.

The structural optimization obtained from computational studies confirms a minimum energy configuration is reached with “piano stool” geometry for all the complexes (Supporting Information Figure S4). The theoretical and experimental bond lengths and angles for complex **3** showed discrepancies lower than 3.15% (Table 2), which allows a more reliable approximation of the predicted bond lengths and angles for complexes **1** and **2**. Minimal changes in angles and bond lengths can

TABLE 2 Experimental for complex **3** and calculated selected bond lengths (\AA) and angles ($^\circ$) for complexes **1**, **2**, and **3**

Geometric parameters	Theoretical (1) (M06) ^b	Theoretical (2) (M06) ^b	Theoretical (3) (M06) ^b	Experimental ^a (3)	Discrepancy theoretical/experimental (3) (%)
Ru1–Cnt ^c	1.7229	1.7305	1.7217	1.6633(10)	3.51
Ru1–Cl1	2.4639	2.4596	2.4626	2.4164(7)	1.91
Ru1–Cl2	2.4590	2.4596	2.4616	2.4179(7)	1.81
Ru–N1	2.2052	2.1895	2.1767	2.174(2)	0.12
Cl1–Ru1–Cl2	90.758	88.281	88.180	86.82(3)	1.57
Cnt–Ru1–Cl1	124.182	126.213	127.152	129.86	-2.08
Cnt–Ru1–Cl2	128.220	127.517	126.518	127.46	-0.74
Cnt–Ru1–N1	129.791	133.630	134.384	131.63	2.09

^aValues for one of the two crystallographically independent molecules.

^bIsolated molecule (in parenthesis, values for the solvated compound).

^cCnt = centroid of the *p*-cymene six-membered ring.

be observed between complexes **1** to **3**. A correlation between the size of the cyclic amine ring and the geometric parameters can be observed. It is worth highlighting the Ru–N1 bond length, which decreases with the increasing number of $-\text{CH}_2$ groups in the amine ring. This characteristic must be related to the higher σ -donor contribution, which establishes a more effective N \rightarrow Ru bond. The similarity between the binding parameters corroborates with the spectroscopic data that predict very similar molecular structures for the three complexes.

The absorption spectra of complexes **1**–**3**, recorded in the 200–800 nm range from CHCl_3 solution (Figure 2), show a high absorption band with λ_{max} at 226 nm ($\epsilon = 1.04 \text{ L mol}^{-1} \text{ cm}^{-1}$) attributed to intraligand transfer of the amine and *p*-cymene. It is also possible to observe

two bands with λ_{max} at 338 ($\epsilon = 0.33 \text{ L mol}^{-1} \text{ cm}^{-1}$) and 408 nm ($\epsilon = 0.26 \text{ L mol}^{-1} \text{ cm}^{-1}$), probably assignable to d \rightarrow π^* charge transfer transitions. The spectra profiles of complexes **1**–**3** are very similar, suggesting quite similar geometric structures for these compounds.

The calculated transitions show good agreement with the experimental values of electronic absorption and the molecular orbitals associated with the transitions present in complexes **1**–**3** are shown in Supporting Information Figure S5. The band at 337 nm comes from two major transitions, HOMO-2 \rightarrow LUMO and HOMO-1 \rightarrow LUMO +1, while three transitions are responsible for the band at 408 nm, HOMO-2 \rightarrow LUMO+1, HOMO-1 \rightarrow LUMO, and HOMO \rightarrow LUMO+1. All of these involve molecular orbitals associated with metal-to-ligand charge transfer

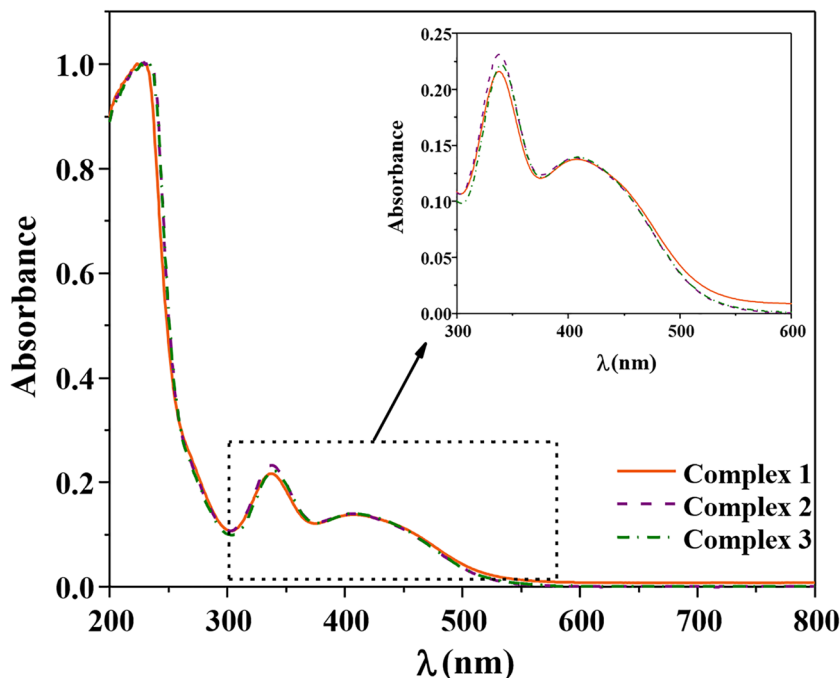


FIGURE 2 Electronic spectra of complexes **1**–**3** from CHCl_3 solution at 25°C ($[\text{Ru}] = 0.1 \text{ mmol/L}$)

(MLCT) from the ruthenium center to the *p*-cymene ligand, while a shoulder at 454 nm is assigned to the HOMO → LUMO transition.

In order to evaluate the electrochemical properties of complexes **1–3**, the redox potentials of the complexes were measured by cyclic voltammetry. The measurement was carried out from CH₂Cl₂ solutions at 25°C using *n*-Bu₄NPF₆ 0.1 M as supporting electrolyte. The cyclic voltammograms of **1–3** are shown in Figure 3 and results are summarized in Table 3. The $E_{1/2}$ values for complexes **1–3** were quite similar, revealing that the difference in the number of methylene groups (CH₂) in the amine ligands does not make a significant contribution to the electron density in the {(*p*-cymene)RuCl₂} moiety. On scanning anodically and reversing the scan direction, all complexes showed waves corresponding to the Ru^{III/II} interconversion. The electrochemical reversibility of the Ru^{II/III} redox pair for ruthenium-catalyzed ATRP is extremely important to support the reversible-deactivation radical polymerization mechanism. Thus, the electrochemical reversibility of complexes **1–3** was initially evaluated by calculating the potential difference (ΔE_p) values and comparing them with the ΔE_p of the ferrocene as the reference obtained under the same experimental conditions. Since complexes **1–3** showed ΔE_p values lower than that of ferrocene, the electrochemical processes are characterized as reversible. Another criterion for reversibility is that the anode/cathode peak current ratio should be close to 1 and independent of the scan rate. This reversibility criterion was calculated for complexes **1–3** at different scanning rates (Supporting

Information Figure S6, left), and the I_{ap}/I_{cp} values were quite close to that expected for a reversible process ($I_{ap}/I_{cp} = 1$). The graphs of I_{cp} and I_{ap} as a function of the square root of the scanning velocity are shown in Supporting Information Figure S6 (right). For a reversible process, the potential sweep velocity affects the I_p , and a linear relationship between I_p and $v^{1/2}$ is expected. Dependence of the current as a function of the square root of the sweep speed was evaluated for complexes **1–3**, and a linearity between I_p and $v^{1/2}$ was obtained. Therefore, the cyclic voltammograms of complexes **1–3** are typical for reversible diffusion-controlled processes.

3.1 | ROMP reactions

Initially, the catalytic activity of the arene–Ru^{II} complexes bearing cyclic amines was evaluated in different [NBE]/[EDA]/[Ru] molar ratios in ROMP reactions. The polymerizations were also performed at 25 and 50°C and in the time range 5–60 min (Scheme 2).

The dependence of yield as a function of time (5–60 min) for ROMP of NBE using complexes **1–3** as catalytic precursors is shown in Figure 4. The influence of time was evaluated using [NBE]/[Ru] = 5000 and [EDA]/[Ru] = 28 in CHCl₃ at 25°C. The increase in time (5–60 min) produced higher yields of polyNBE, reaching 64% yield in 60 min for complex **3**. The polyNBE obtained using these complexes showed an increase in the molecular weight (M_n) as the reaction time increased, followed by a decrease in polydispersity index (PDI) values (Supporting Information Figure S7).

The activity of complexes **1–3** was also tested at 50°C under the same conditions. Although the yields presented a subtle increase, the polyNBEs exhibited bimodal molecular weight distributions (Supporting Information Figure S8). In general, a low temperature favors the thermodynamics of polymerization, but discourages the kinetics of the induction period. Furthermore, the use of a minimum temperature is necessary to promote the formation of active species (Ru–carbene). Considering that the catalytic activity of complexes **1–3** remained practically the same at 50°C, it is possible to infer that the induction period has no temperature dependence to initiate the ROMP. The catalytic activity was shown to be sensitive to the [EDA]/[Ru] ratio, with an increase in the yield up to [EDA]/[Ru] = 28, followed by an abrupt drop for [EDA]/[Ru] > 28, when using [NBE]/[Ru] = 5000 for 60 min at 25°C (Supporting Information Figure S9); no reaction was observed in the absence of EDA. Considering that complexes **1–3** have a similar profile when reacted with EDA, it is possible to suggest that the three complexes

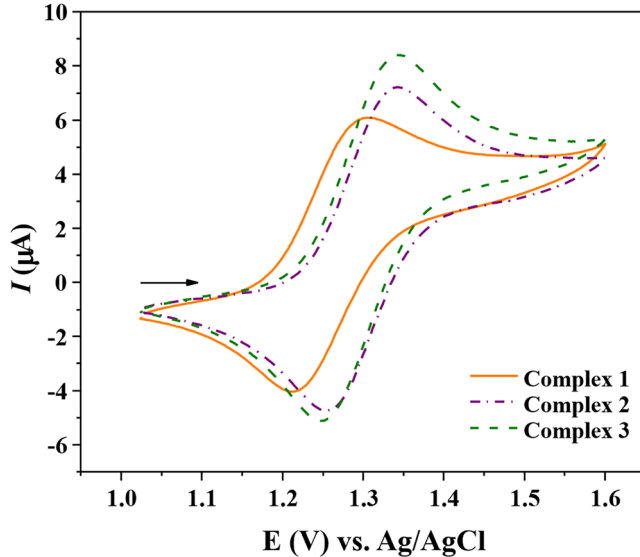
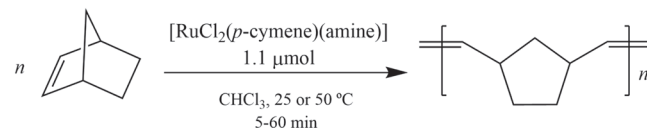


FIGURE 3 Cyclic voltammograms of complexes **1–3** from CH₂Cl₂ solution at 25°C. Scanning anodically from 1.0 to 1.6 V at scan rate of 100 mV/s. [Ru] = 1.0 mmol/L; [*n*-Bu₄NPF₆] = 0.1 mol/L

TABLE 3 Cyclic voltammetry results for complexes **1–3**

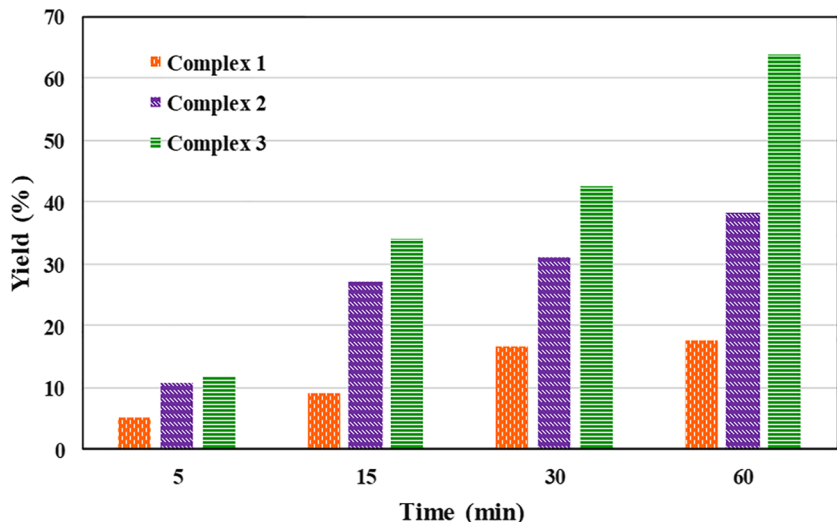
Compound	E_{ap} (V)	E_{cp} (V)	$E_{1/2}^a$ (V)	ΔE_p^b (V)	I_{ap}/I_{cp}
1	1.31	1.21	1.26	0.10	1.03
2	1.34	1.25	1.29	0.09	1.05
3	1.34	1.24	1.29	0.10	1.06
Ferrocene	0.58	0.34	0.46	0.24	1.09

^a $E_{1/2} = (E_{ap} + E_{cp})/2$.^b $\Delta E_p = E_{ap} - E_{cp}$.**SCHEME 2** ROMP of NBE catalyzed by complexes **1–3**

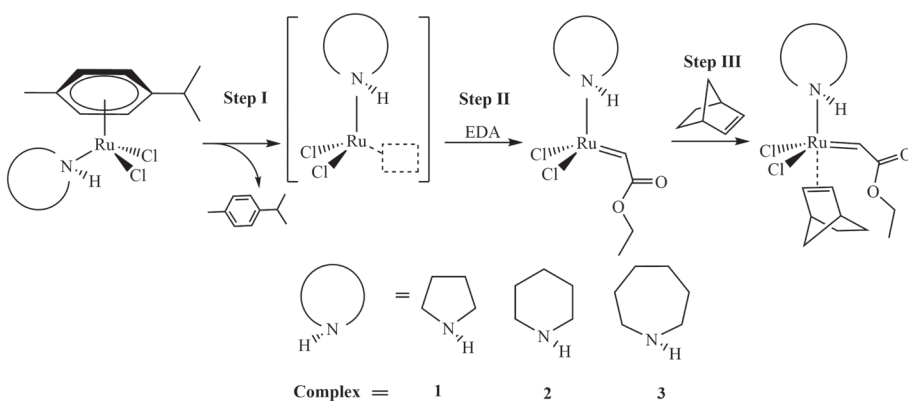
have the same pathway in the formation of Ru–carbene in the induction period. With an excessive amount of EDA ($[EDA]/[Ru] > 28$), the decreasing in the yields and molecular weight values can be associated with secondary reactions (Supporting Information Figure S10).^[23] Consequently, the large amount of EDA interferes in the dynamic of the ROMP reaction (initiation and propagation) and as a result low yields and broad PDIs are obtained. The effect of the $[NBE]/[Ru]$ ratio on the yield of the isolated polymers follows an increase in the yield values to $[NBE]/[Ru] = 5000$, followed by a decreasing of the yields to saturation curve profile (Supporting Information Figure S11), when using $[EDA]/[Ru] = 28$ for 60 min at 25°C. The yield rose to 18–64% when the $[NBE]/[Ru]$ ratio was increased from 1000 to 5000. For $[NBE]/[Ru] > 5000$, a decrease in the yield and molecular weight was observed (Supporting Information Figure S12) and this can be associated with the cage effect, which hinders the approach of the monomer to the metal center.^[23]

Evaluating the catalytic activity for ROMP of NBE, the following order of reactivity was observed when the activity of the complexes was compared: **3** > **2** > **1**. This order of activity could be predominantly associated with steric reasons, although the higher Ru → olefin synergism, given by the σ-donor characteristic of the amine ligands, also plays as an important role in ROMP activity.

A kinetic study of complexes **1–3** in presence of EDA was monitored by UV–Vis in $CHCl_3$ solution at 25°C to measure the rate of formation of the metathetical species using a $[EDA]/[Ru] = 28$ molar ratio ($[Ru] = 1.0 \times 10^{-5}$ mol/L and $[EDA] = 1.26 \times 10^{-5}$ mol/L) (Supporting Information Figure S13). Analyzing the kinetic behavior of complexes **1–3** in the presence of EDA, great similarity was observed in the absorption spectra profiles over the time. The increase of absorbance followed by bathochromic displacement of the band at 338 nm in the accumulated spectra could be attributed to a change in the coordination sphere of the complexes. The changes in absorption spectra of complexes **1–3** are associated with coordination of the EDA to the Ru center. The kinetic studies also showed a linear correlation of $\ln(A_t - A_{inf})$ as a function of time (Supporting Information Figure S13, insert) with pseudo first-order rate constants (k_{obs}) equal to 6.2×10^{-3} , 4.0×10^{-3} , and 4.4×10^{-3} s⁻¹ for **1**, **2**, and **3**, respectively.

**FIGURE 4** Dependence of yield as a function of time for ROMP of NBE with complexes **1–3**. $[NBE]/[Ru] = 5000$ and $[EDA]/[Ru] = 28$ (5 μL of EDA) in $CHCl_3$ at 25°C

SCHEME 3 Proposal of ROMP mechanism using complexes **1–3** as precatalysts



In the ROMP experiments in the presence of a 20-fold excess of *p*-cymene, the yields of polyNBE were less than 2% of polyNBE, whereas almost no change can be observed in the activity when performed in the presence of amine using [NBE]/[EDA]/[Ru] = 5000/28/1 for 60 min at 25°C. Probably the presence of *p*-cymene in solution suppresses the leaving of the arene ligand, preventing the ROMP reaction. These experiments suggest that the ROMP reaction using complexes **1–3** depends on the lability of the *p*-cymene ligand, considering that the polymerization was inhibited in presence of this molecule. This result is agreement with previous reports using similar compounds, which suggest the labilization of the arene ligand from the ruthenium center in the presence of diazocompound.^[50,51]

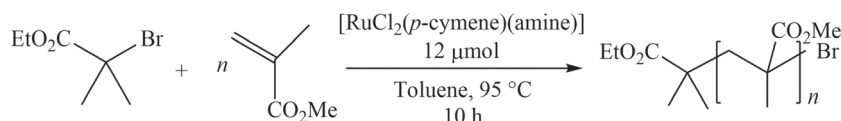
To better understanding the differences in activity between [RuCl₂(*p*-cymene)(amine)] systems, the mechanism from the induction period (metal carbene formation) up to initiation step was examined. Since mechanisms of homogeneous catalysis are usually hard to elucidate due to difficulty in monitoring and controlling the intermediate species that arise, as occurs in the ROMP reaction, it is important to emphasize that the research proposed here is based on the combination of theoretical and experimental results. This approach is more likely to succeed, providing the most plausible path for this reaction. In the two limiting cases, this substitution could take place in an associative or dissociative fashion. As these complexes **1–3** are six-coordinated species, theoretically the ROMP could occur via a dissociative mechanism. An analysis of the thermodynamic parameters calculated from quantum-mechanical data corroborates the dissociation of the *p*-cymene, as suggested by experiments in the presence of this ligand. The obtained values suggest that the mechanism should involve the initial loss of *p*-cymene coordinated to the initial complex, followed by coordination of EDA to the Ru center to generate a 14-electron intermediate (Scheme 3 and Table 4). The EDA coordination to the saturated 18-electron [RuCl₂(*p*-cymene)(amine)]

complexes did not converge, suggesting that the {Ru = CHCO₂Et} bond should not be formed, while the dissociation of *p*-cymene takes place to generate a 14-electron metal carbene intermediate, followed by trapping with the olefinic substrate (Supporting Information Figure S14). In addition, considering that the path that involves the formation of the metathetically active {RuCl₂(amine)(=CHCO₂Et)} via a dissociative mechanism involves several concerted reactions, it is very likely that the overall thermodynamic parameters for the process are favorable. Considering the overall equation [RuCl₂(*p*-cymene)(amine)] + EDA + NBE → {RuCl₂(amine)(=CHCO₂Et)(NBE)} + *p*-cymene and based on the thermodynamic parameters calculated for the individual reactions via the dissociative mechanism, the calculated thermodynamical parameters for the overall reaction can be estimated (Table 4). These data suggest that the formation of the {RuCl₂(amine)(=CHCO₂Et)(NBE)} via a dissociative mechanism is thermodynamically favorable in all cases (Scheme 3).

Comparing the yields for ROMP of norbornene with the complexes of type [RuCl₂(L)(amine)], where L = PPh₃ or *p*-cymene, a similar behaviour using the same amines is observed.^[52–54] However, the phosphine–amine complexes produced higher yields. It was demonstrated by calculation and kinetic studies via FT-IR that

TABLE 4 Calculated thermodynamic parameters associated with the reaction of EDA and NBE with complexes **1–3** at 298 K

		1	2	3
Step I	ΔG (kJ/mol)	101.99	165.24	109.18
	ΔH (kJ/mol)	251.12	227.63	180.25
Step II	ΔG (kJ/mol)	−325.54	−280.07	−281.32
	ΔH (kJ/mol)	−386.63	−338.46	−344.79
Step III	ΔG (kJ/mol)	2.91	−7.65	32.84
	ΔH (kJ/mol)	−45.11	59.86	−14.93
Overall	ΔG (kJ/mol)	−130.73	−122.61	−139.30
	ΔH (kJ/mol)	−180.61	−170.69	−191.56



S C H E M E 4 ATRP of MMA catalyzed by complexes **1–3**

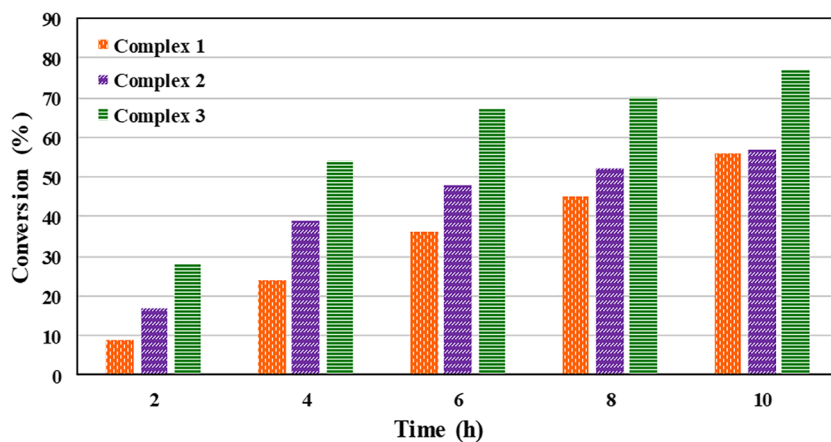


FIGURE 5 Dependence of conversion on the reaction time for ATRP of MMA with complexes **1–3**. [MMA]/[EBiB]/[Ru] = 1000/2/1 with 12 μmol of complex in toluene at 95°C

the phosphine–amine complexes react first with EDA, losing the phosphine ligands, followed by the reaction with monomer.^[55,56] As these phosphine–amine complexes are 16-electron species, they undergo efficient substitution processes. On the other hand, as the *p*-cymene ligand is a six-electron donor and the *p*-cymene–amine complexes are 18-electron species, reactions with EDA

via dissociative substitution, as here demonstrated, would be difficult.

3.2 | ATRP reactions

We investigated the catalytic activity of the arene–Ru^{II} complexes (**1–3**) in the direct ATRP of MMA. Initially,

T A B L E 5 Conversion values and GPC data from the ATRP of MMA with **1–3**: [MMA]/[EBiB]/[Ru] = 1000/2/1 with 12 μmol of complex in toluene at 95°C

Complex	Time ^a (hr)	Conversion ^b (%)	M _{n,exp} ^c (10 ⁴ g/mol)	M _{n,theor} ^d (10 ⁴ g/mol)	PDI ^c
1	2	9.07	3.16	0.45	2.16
	4	24.63	3.23	1.23	2.14
	6	36.69	3.30	1.84	1.96
	8	45.12	3.56	2.26	2.05
	10	56.39	3.80	2.82	1.66
2	2	17.46	2.67	0.35	2.10
	4	39.65	2.75	1.98	1.79
	6	48.82	2.91	2.44	1.68
	8	52.08	3.14	2.60	1.49
	10	57.49	3.78	2.87	1.37
3	2	28.76	15.42	1.43	2.46
	4	54.73	23.91	2.74	1.95
	6	67.34	30.16	3.37	1.61
	8	70.19	34.60	3.51	1.53
	10	77.53	34.97	3.88	1.98

^a[MMA]/[EBiB]/[Ru] = 1000/2/1. ^bDetermined by GC. ^cDetermined by GPC in THF. ^dM_{n,teor} = [MMA]/[EBiB] × M_{w,MMA} × conversion.

the reaction conditions were varied and optimized. The optimal temperature was found to be 95°C, whereas lower temperatures resulted in a decrease in the conversion without an increase in the quality of the polymer obtained. The best [MMA]/[EBiB]/[Ru] ratio was determined as 1000/2/1 (Scheme 4). Figure 5 shows the conversion results obtained with the three complexes and the molecular weight data are summarized in Table 5. Since ATRP is based on a redox equilibrium between a dormant species and an active species, the redox pair Ru^{III}/Ru^{II} of the catalysts should be accessible as determined by cyclic voltammetry. MMA conversion values for all complexes increased as a function of time with complexes **1**, **2**, and **3** reaching 56%, 57%, and 77% within 10 hr, respectively.

The plot of $\ln([MMA]_0/[MMA]_t)$ as a function of reaction time shows an asymptotic relationship for all catalysts, revealing that the radical concentration is not constant during MMA polymerization. The polyMMA molecular weights of the order of 10⁴ g/mol obtained with complexes **1–3** increased as a function of MMA conversion (Table 5). The GPC curves of the polyMMAs show a monomodal distribution and shift to higher values with conversion (Supporting Information Figure S15); however, the molecular weights are much higher than those theoretically predicted in all cases, suggesting the existence of considerable termination. It should be noted that the values of the polydispersity index and molecular weights are modest in comparison with those found in the literature for other systems.^[24] Although the controlling ability was poor, the sustained polymerization and the M_n growth with conversion demonstrate the reversibility of atom transfer in the ATRP equilibrium.

4 | CONCLUSIONS

Complexes **1–3** were successfully synthesized and characterized by elemental analysis, FT-IR, UV-Vis, and ¹H and ¹³C{¹H} NMR spectroscopy. The electrochemistry properties of complexes **1–3** were investigated by cyclic voltammetry and exhibited two successive single-electron oxidation processes. Complexes **1–3** demonstrated better catalytic activities as precatalysts in ROMP of NBE at 50°C with [NBE]/[Ru] ratio of 5000 in the presence of 5 µl of EDA for 5–60 min. Complex **3** exhibited better performance in ROMP reactions. The catalytic activity of complexes **1–3** in ROMP increased as the CH₂ group increased in the cyclic amine. The polymerization of MMA mediated by complexes **1–3** was performed using a [MMA]/[EBiB]/[Ru] = 1000/2/1 molar ratio at 95°C. These complexes display some activity as mediators for the controlled radical polymerization of MMA following

an ATRP mechanism. Nevertheless, the level of control achieved was modest and only slightly dependent on the structure of the amine ligand.

ACKNOWLEDGMENTS

VPCJ and BSLN are indebted to the financial support from FAPESP, Proc. 2018/06340-1 and Proc. 2017/06329-5, respectively. This work was supported by the Coordenação de Aperfeiçoamento de Pessoal de Nível Superior – Brasil (CAPES) – Finance Code 001.

ORCID

Pedro Ivo S. Maia <https://orcid.org/0000-0003-4699-9481>

Valdemiro P. Carvalho-Jr <https://orcid.org/0000-0001-8843-2841>

REFERENCES

- [1] R. Poli, *Angew Chem Int Ed* **2006**, *45*, 5058.
- [2] R. Poli, *Eur. J. Inorg. Chem.* **2011**, *10*, 1513.
- [3] M. Kamigaito, T. Ando, M. Sawamoto, *Chem. Rev.* **2001**, *101*, 3689.
- [4] K. Matyjaszewski, J. H. Xia, *Chem. Rev.* **2001**, *101*, 2921.
- [5] F. di Lena, K. Matyjaszewski, *Prog. Polym. Sci.* **2010**, *35*, 959.
- [6] N. V. Tsarevsky, K. Matyjaszewski, *Chem. Rev.* **2007**, *107*, 2270.
- [7] K. Matyjaszewski, *Macromolecules* **2012**, *45*, 4015.
- [8] K. Matyjaszewski, N. V. Tsarevsky, *Nat. Chem.* **2009**, *1*, 276.
- [9] C. W. Bielawski, R. H. Grubbs, *Prog. Polym. Sci.* **2007**, *32*, 1.
- [10] K. Nomura, M. M. Abdellatif, *Polymer* **2010**, *51*, 1861.
- [11] D. Yang, W. Huang, J. H. Yu, J. S. Jiang, L. Y. Zhang, M. R. Xie, *Polymer* **2010**, *51*, 5100.
- [12] L. C. So, S. Faucher, S. Zhu, *Prog. Polym. Sci.* **2014**, *39*, 1196.
- [13] M. Kamigaito, *J Polym* **2011**, *43*, 105.
- [14] A. Demonceau, A. F. Noels, E. Saive, A. J. Hubert, *J. Mol. Catal.* **1992**, *76*, 123.
- [15] L. Delaude, A. Demonceau, A. F. Noels, *Curr. Org. Chem.* **2006**, *10*, 203.
- [16] (a)A. W. Stumpf, E. Saive, A. Demonceau, A. F. J. Noels, *Chem Soc Chem Commun* **1995**, 1127. (b)A. Demonceau, A. W. Stumpf, E. Saive, A. F. Noels, *Macromolecules* **1997**, *30*, 3127.
- [17] A. Hafner, A. Mühlbach, P. A. van der Schaaf, *Angew Chem Int Ed Engl* **1997**, *36*, 2121.
- [18] (a)R. Drozdak, B. Allaert, N. Ledoux, I. Dragutan, V. Dragutan, F. Verpoort, *Coord. Chem. Rev.* **2005**, *249*, 3055. (b)K. C. Gupta, A. K. Sutar, *Coord. Chem. Rev.* **2008**, *252*, 1420.
- [19] (a)T. Opstal, K. Couchez, F. Verpoort, *Adv Synth Catal* **2003**, *345*, 393. (b)B. D. Clercq, F. Verpoort, *J. Mol. Catal. A: Chem.* **2002**, *180*, 67.
- [20] (a)L. Delaude, A. Demonceau, A. F. Noels, *Chem Commun* **2001**, 986. (b)L. Delaude, M. Szypa, A. Demonceau, A. F. Noels, *Adv Synth Catal* **2002**, *344*, 749. (c)Y. Zhang, D. Wang, P. Lönnecke, T. Scherzer, M. R. Buchmeiser, *Macromol. Symp.* **2006**, *236*, 30. (d)M. R. Buchmeiser, D. Wang, Y. Zhang, S. Naumov, K. Wurst, *Eur. J. Inorg. Chem.* **2007**, 3988.

- [21] (a) N. Ledoux, B. Allaert, F. Verpoort, *Eur. J. Inorg. Chem.* **2007**, 5578. (b) L. Delaude, S. Delfosse, A. Richel, A. Demonceau, A. F. Noels, *Chem Commun* **2003**, 1526. (c) J. Baraut, A. Massard, F. Chotard, E. Bodio, M. Picquet, P. Richard, P. Le Gendre, *Eur. J. Inorg. Chem.* **2015**, 16, 2671.
- [22] T. R. Cruz, R. A. N. Silva, A. E. H. Machado, B. S. Lima-Neto, B. E. Goi, V. P. Carvalho-Jr, *New J. Chem.* **2019**, 43, 6220.
- [23] L. R. Fonseca, J. L. Silva Sá, V. P. Carvalho, B. S. Lima-Neto, *Polym. Bull.* **2018**, 32, 1.
- [24] A. H. S. Idehara, P. D. S. Gois, H. Fernandes, B. E. Goi, A. E. H. Machado, B. S. Lima-Neto, V. P. Carvalho-Jr, *Mol Cat* **2018**, 448, 135.
- [25] M. S. Ferreira, H. Fernandes, J. L. S. Sá, V. P. Carvalho-Jr, B. S. Lima-Neto, *Pol Bulletin* **2018**, 75, 1.
- [26] M. B. A. Afonso, L. G. Gonçalves, T. T. Silva, J. L. S. Sá, N. C. Batista, B. E. Goi, V. P. Carvalho-Jr, *Polímeros: Ciência e Tecnologia* **2018**, 28, 1.
- [27] R. A. N. Silva, P. Borim, L. R. Fonseca, B. S. Lima-Neto, J. L. Silva Sá, V. P. Carvalho-Jr, *Cat Letters* **2017**, 147, 1144.
- [28] M. B. A. Afonso, T. R. Cruz, Y. F. Silva, J. C. A. Pereira, A. E. H. Machado, B. E. Goi, B. S. Lima-Neto, V. P. Carvalho-Jr, *J Org Chem* **2017**, 851, 225.
- [29] P. Borim, B. S. Lima-Neto, B. E. Goi, V. P. Carvalho Jr., *Inorg. Chim. Acta* **2017**, 456, 171.
- [30] T. R. Cruz, P. Borim, B. E. Goi, J. L. Silva Sá, B. S. Lima-Neto, V. P. Carvalho-Jr, *J Pol Res* **2017**, 24, 13.
- [31] C. P. Ferraz, L. R. Fonseca, V. Tomazetti, F. C. Silva, B. S. Lima-Neto, V. P. Carvalho Jr., *New J. Chem.* **2016**, 32, 01.
- [32] M. B. Afonso, L. Gonçalves, P. Borim, J. L. Silva Sá, B. E. Goi, V. P. Carvalho-Jr, *J. Chem Soc* **2016**, 28, 1407.
- [33] H. K. Chaves, C. P. Ferraz, V. P. Carvalho, B. S. Lima-Neto, *J Mol Cat a Chem* **2014**, 385, 46.
- [34] V. P. Carvalho Jr., C. P. Ferraz, B. S. Lima-Neto, *Inorg. Chim. Acta* **2014**, 418, 1.
- [35] V. P. Carvalho Jr., C. P. Ferraz, J. L. Silva Sá, B. S. Lima-Neto, *Quím Nova (Imp)* **2012**, 35, 791.
- [36] V. P. Carvalho Jr., C. P. Ferraz, B. S. Lima-Neto, *Eur. Polym. J.* **2011**, 47, 837.
- [37] S. A. A. Santana, V. P. Carvalho Jr., B. S. Lima-Neto, *J. Venom, Anim. Toxins incl. Trop. Dis.* **2010**, 21, 279.
- [38] V. P. Carvalho Jr., C. P. Ferraz, B. S. Lima-Neto, *J Mol Cat a Chem* **2010**, 333, 46.
- [39] D. M. Martins, P. I. S. Maia, V. P. Carvalho-Jr., B. S. Lima-Neto, *Eur. J. Inorg. Chem.* **2019**, 2019(41), 4421.
- [40] T. B. Silva, D. M. Martins, P. D. S. Gois, P. Borim, P. I. S. Maia, V. P. Carvalho Jr., B. S. Lima-Neto, *Inorg Chem Comm* **2020**. <https://doi.org/10.1016/j.inoche.2019.107749>
- [41] M. A. Bennett, T. N. Huang, T. W. Matheson, A. K. Smith, *Inorg Synt* **1982**, 21.
- [42] G. M. Sheldrick, *SADABS*, University Göttingen, Germany **2014**.
- [43] G. M. Sheldrick, *Acta Crystallogr Sect a* **2015**, 71, 3.
- [44] G. M. Sheldrick, *Acta Crystallogr Sect C* **2015**, 71, 3.
- [45] L. J. Farrugia, *J. Appl. Crystallogr.* **2012**, 45, 849.
- [46] Y. Zhao, D. G. Truhlar, *Theor Chem Account* **2006**, 120, 215.
- [47] M. J. Frisch, G. W. Trucks, H. B. Schlegel, G. E. Scuseria, M. A. Robb, J. R. Cheeseman, G. Scalmani, V. Barone, B. Mennucci, G. A. Petersson, H. Nakatsuji, M. Caricato, X. Li, H. P. Hratchian, A. F. Izmaylov, J. Bloino, G. Zheng, J. L. Sonnenberg, M. Hada, M. Ehara, K. Toyota, R. Fukuda, J. Hasegawa, M. Ishida, T. Nakajima, Y. Honda, O. Kitao, H. Nakai, T. Vreven, J. A. Montgomery Jr., J. E. Peralta, F. Ogliaro, M. Bearpark, J. J. Heyd, E. Brothers, K. N. Kudin, V. N. Staroverov, T. Keith, R. Kobayashi, J. Normand, K. Raghavachari, A. Rendell, J. C. Burant, S. S. Iyengar, J. Tomasi, M. Cossi, N. Rega, J. M. Millam, M. Klene, J. E. Knox, J. B. Cross, V. Bakken, C. Adamo, J. Jaramillo, R. Gomperts, R. E. Stratmann, O. Yazyev, A. J. Austin, R. Cammi, C. Pomelli, J. W. Ochterski, R. L. Martin, K. Morokuma, V. G. Zakrzewski, G. A. Voth, P. Salvador, J. J. Dannenberg, S. Dapprich, A. D. Daniels, O. Farkas, J. B. Foresman, J. V. Ortiz, J. Cioslowski, D. J. Fox, *Gaussian 09, Revision E.01*, Gaussian, Inc., Wallingford CT **2013**.
- [48] N. Godbout, D. R. Salahub, J. Andzelm, E. Wimmer, *Can. J. Chem.* **1992**, 70, 560.
- [49] J. Tomasi, B. Mennucci, E. Cancès, *J. Mol. Struct.: THEOCHEM* **1999**, 464, 211.
- [50] A. Demonceau, A. W. Stumpf, E. Saive, A. F. Noels, *Macromolecules* **1997**, 30, 3127.
- [51] L. Delaude, X. Sauvage, A. Demonceau, J. Wouters, *Organometallics* **2009**, 28, 4056.
- [52] J. M. E. Matos, B. S. Lima-Neto, *J Mol Cat a: Chem* **2004**, 222, 81.
- [53] J. L. Silva Sá, L. H. Vieira, E. S. P. Nascimento, B. S. Lima-Neto, *Applied Cat a: Gen* **2010**, 374, 194.
- [54] L. R. Fonseca, E. S. P. Nascimento, J. L. Silva Sá, B. S. Lima-Neto, *New J. Chem.* **2015**, 39, 4063.
- [55] R. J. Fernandes, T. B. Silva, B. S. Lima-Neto, R. L. A. Haiduke, *J. Mol. Catal. A: Chem.* **2015**, 410, 58.
- [56] V. K. Tomazett, W. G. Santos, B. S. Lima-Neto, *Reac Kinet Mech Cat* **2017**, 120, 663.

SUPPORTING INFORMATION

Additional supporting information may be found online in the Supporting Information section at the end of this article.

How to cite this article: Cruz TR, Silva EA, Oliveira DP, et al. Dual catalytic performance of arene-ruthenium amine complexes for norbornene ring-opening metathesis and methyl methacrylate atom-transfer radical polymerizations. *Appl Organometal Chem.* 2020;e5602. <https://doi.org/10.1002/aoc.5602>